Journal of Biomolecular Structure and Dynamics

ISSN: (Print) (Online) Journal homepage: https://www.tandfonline.com/loi/tbsd20

A molecular dynamics investigation of N-glycosylation effects on T-cell receptor kinetics

Zachary Rollins, Bradley Harris, Steven George & Roland Faller

To cite this article: Zachary Rollins, Bradley Harris, Steven George & Roland Faller (2022): A molecular dynamics investigation of N-glycosylation effects on T-cell receptor kinetics, Journal of Biomolecular Structure and Dynamics, DOI: 10.1080/07391102.2022.2091660

To link to this article: https://doi.org/10.1080/07391102.2022.2091660

View supplementary material

Published online: 28 Jun 2022.

Submit your article to this journal

Article views: 110

View related articles

View Crossmark data

Full Terms & Conditions of access and use can be found at
https://www.tandfonline.com/action/journalInformation?journalCode=tbsd20

JOURNAL OF BIOMOLECULAR STRUCTURE AND DYNAMICS
https://doi.org/10.1080/07391102.2022.2091660

Taylor & Francis
Taylor & Francis Group

Check for updates

A molecular dynamics investigation of N-glycosylation effects on T-cell receptor kinetics

Zachary Rollins[a], Bradley Harris[a], Steven George[b] and Roland Faller[a]

[a]Department of Chemical Engineering, University of California, Davis, Davis, CA, USA; [b]Department of Biomedical Engineering, University of California, Davis, Davis, CA, USA

Communicated by Ramaswamy H. Sarma

ABSTRACT

The binding interaction between the T-cell receptor (TCR) and peptide-major histocompatibility complex (pMHC) is modulated by several factors (known and unknown), however, investigations into effects of glycosylation are limited. A fully glycosylated computational model of the TCR bound to the pMHC is developed to investigate the effects of glycosylation on dissociation kinetics from the pMHC. Here, we examine the effects of N-glycosylation on TCR-pMHC bond strength using steered molecular dynamic simulations. N-glycosylation is a post-translational modification that adds sugar moieties to molecules and can modulate the activity of several immune molecules. Using a TCR-pMHC pair found in melanoma as a case study, our study demonstrates that N-glycosylation of the TCR-pMHC alters the proteins' conformation; increases the bond lifetime; and increases the number of hydrogen bonds and Lennard-Jones Contacts involved in the TCR-pMHC bond. We find that weak glycan-protein or glycan-glycan interactions impact the equilibrated structure of the TCR and pMHC leading to an increase in the overall bond strength of the TCR-pMHC complex including the duration and energetic strength under constant load. These results indicate that N-glycosylation plays an important role in the TCR-pMHC bond and should be considered in future computational and experimental studies.

ARTICLE HISTORY
Received 9 May 2022
Accepted 13 June 2022

KEYWORDS
Glycosylation; MD simulation; TCR receptor

Introduction

N-glycosylation is a post-translational modification that is required for the normal function of many immune molecules (Marth & Grewal, 2008). Alterations in glycosylation patterns are known to influence protein expression, function, and signaling in several immune pathways (Lyons et al., 2015)—including the development, selection, and activation of T cells (Bousser et al., 2020). The T-cell receptor (TCR) is central in the ability of a T cell to discriminate peptide-major histocompatibility complexes (pMHCs)—a substantial feature of the adaptive immune response—and modifications to glycosylation patterns likely affect these binding interactions (Clark & Baum, 2012). Glycosidic linkages are constructed almost exclusively from ten monosaccharide building blocks by a multiplicity of enzymes in the endoplasmic reticulum and golgi apparatus (Schjoldager et al., 2020). The exact glycan synthesis and regulation pathways are not completely understood; however, the glycome is known to be cell-type specific and dynamic in response to cues throughout development, differentiation, and activation (Bousser et al., 2020). Post-translational additions of N-glycan chains to the TCR modify the T-cell activation threshold (Cerliani et al., 2016; Gómez-Henao et al., 2021; Rabinovich & Toscano, 2009). For example, modification of N-Glycosylation has been shown to promote the antitumor immune response of human T cells (Sasawatari et al., 2020). More specifically, the treatment of T cells with 2-deoxy-D-glucose (2DG)—an N-Glycosylation modulator– enhances the antitumor activity of T cells (Sasawatari et al., 2020). Thus, administration of 2DG during *ex vivo* expansion of T cells has been suggested for T cell-based immunotherapies as a metabolic reprogramming tool. 2DG treated human T cells demonstrate a 10-15 fold increase in the relative expression of deoxyhexose-containing *N*-glycans measured by MALDI-TOF mass spectrometry (Sasawatari et al., 2020). The atomic-level effect of these glycans on the TCR-pMHC interaction is currently unknown.

The relative motion of glycans (∼1 kDa) is faster than that of proteins (∼50 kDa), making the structural changes caused by glycans on proteins challenging to resolve experimentally (Petrescu et al., 1999). Due to the fast dynamics of glycans, uncovering realistic equilibrated glycan conformations can be readily achieved utilizing atomistic molecular dynamic (MD) simulations. Algorithms to attach glycans to proteins have led to only a limited set of fully glycosylated protein structures (Bernardi et al., 2017, 2019, 2020; Grant et al., 2020; Harbison & Fadda, 2020; Jo et al., 2015; Lu et al., 2012; Woo et al., 2020; Xiong et al., 2019; Yanaka et al., 2019) and our group has made significant progress in glycan modelling (Bernardi et al., 2017, 2019; Huang et al., 2022). Herein, we investigate the effects of glycosylation on the structure of

CONTACT Roland Faller rfaller@ucdavis.edu Department of Chemical Engineering, University of California, Davis, Kemper Hall, Davis, CA 95616, USA.
Supplemental data for this article can be accessed online at http://dx.doi.org/10.1080/07391102.2022.2091660
© 2022 Informa UK Limited, trading as Taylor & Francis Group

the T Cell Receptor (Figure 1) and the impact on TCR-pMHC bond strength (Figure 2).

Methods

N-glycosylation

The crystal structure of the DMF5 TCR bound to the MART1 peptide – HLA-A2 complex (pMHC) was used as the base structure (Borbulevych et al., 2011; Rollins et al.). To investigate the effects of N-glycosylation on the TCR-pMHC binding interaction, we employed the Glycam server (Group of Robert J. Woods, XXXX) to attach the deoxyhexose containing N-glycan, DGalpb1-4DGlcpNAcb1-2DManpa1-6[DGalpb1-4DGlcpNAcb1-2DManpa1-3]DManpb1-4DGlcpNAcb1-4[LFucpa1-6]DGlcpNAcb1-OME, to all of the DMF5 TCR (PDB ID: 3QDJ) N-glycosylation sites: N405, N497, N560, N568, and N765 (Sasawatari et al., 2020) (Figure 1). Although we only investigated one N-glycan on the TCR, this deoxyhexose contain N-glycan has been reported to be expressed ~15-fold higher in 2DG treated T cells (Sasawatari et al., 2020). Thus, this study serves as an initial exploration of the effect of a glycan, with known augmentation of T-cell activation, on the TCR-pMHC binding interaction. Additionally, we attached the high mannose glycan, DManpa1-2DManpa1-6[DManpa1-2DManpa1-3]DManpa1-6[DGlcpa1-3DGlcpa1-3DManpa1-2DManpa1-2DManpa1-3]DManpb1-4DGlcpNAcb1-4DGlcpNAcb1-OH, to site N86 (Ryan & Cobb, 2012; Wooster & Anderson, 2019) of the MART1 pMHC (HLA-A2) which is bound to the DMF5 TCR (Figure 1). N-glycosylation sites were predicted by the triplet motif standard: asparagine—*X*—threonine/serine (*X* is any amino acid except proline) (Bause, 1983). Then, glycans are attached to the asparagine residues (N) that comply with the triplet motif standard. The topology files were then generated using AmberTools (Case et al., 2016) and converted to Gromacs format using Acpype (Bernardi et al., 2019; Sousa da Silva & Vranken, 2012). Next, a rigid bond rotation of the glycans was performed to achieve a minimized *in vacuo* energy configuration utilizing GlyRot (Bernardi, 2020) (Figure 2).

Molecular dynamics setup

The effect of glycosylation on the TCR-pMHC structure was evaluated by comparing the aglycosylated and glycosylated structures (Figure 1). Interfacial substructures were defined by sequential residues from the corresponding chains: TCRα (CDR1α: 407-415, CDR2α: 433-438, CDR3α: 472-482), TCRβ (CDR1β: 607-613, CDR2β: 630-637, CDR3β: 674-685), MHCα (MHCβ: 50-85, MHCα: 138-179), and peptide (MART1: 375-383). Moreover, glycans are assigned sequential residues on the TCR (DGalpb1-4DGlcpNAcb1-2DManpa1-6[DGalpb1-4DGlcpNAcb1-2DManpa1-3]DManpb1-4DGlcpNAcb1-4[LFucpa1-6]DGlcpNAcb1-OME: 858-887) and MHCα (DManpa1-2DManpa1-6[DManpa1-2DManpa1-3]DManpa1-6[DGlcpa1-3DGlcpa1-3DManpa1-2DMan pa1-2DManpa1-3]DManpb1-4DGlcpNAcb1-4DGlcpNAcb1-OH: 845-857), respectively. To determine protonation states, pK_a values were calculated using propka3.1 (Olsson et al., 2011; Søndergaard et al., 2011) and residues were considered deprotonated in Gromacs (Van Der Spoel et al., 2005) if pK_a values were below the physiologic 7.4 pH (Figure 2). The resulting systems were solvated in rectangular water boxes using the SPC/E water model (Berendsen et al., 1987) large enough to satisfy the minimum image convention. Na^+ and Cl^- ions were added to neutralize protein charge and reach physiologic salt concentration ~150 mM. All simulations were performed with Gromacs 2019.1 (Van Der Spoel et al., 2005) using the AmberFF14SB forcefield for protein atoms (Maier et al., 2015), Glycam06-j forcefield for glycan atoms(Kirschner et al., 2008), and orthorhombic periodic boundary conditions. All simulations were in atomistic detail (Table 1).

Energy minimization and equilibration

Generating equilibrated starting structures for the steered molecular dynamics simulations required seven steps. (Marth & Grewal, 2008) Steepest descent energy minimization to ensure correct geometry and the absence of steric clashes (emtol = 1000 kJ/mol/nm). (Lyons et al., 2015) Solvate and add neutralizing/physiologic concentration of Na^+ Cl^- ions. (Bousser et al., 2020) 10 ps simulation in the constant volume ensemble (NVT) with 0.2 fs timestep ($T = 310$ K) to relax solute-solvent contacts (Clark & Baum, 2012). Steepest descent energy minimization (emtol = 1000 kJ/mol/nm). (Schjoldager et al., 2020) 100 ps simulation in the constant volume (NVT) ensemble with 2 fs timestep to bring atoms to correct kinetic energies. A temperature of 310 K was maintained by coupling all protein and nonprotein atoms in separate baths using the velocity rescaled thermostat and a 0.1 ps time constant (Berendsen et al., 1984; Cerliani et al., 2016) 100 ps simulation in the constant pressure (NPT) ensemble using Berendsen pressure coupling(Berendsen et al., 1984) and a 2.0 ps time constant to maintain isotropic pressure at 1.0 bar (2 fs timestep). (Rabinovich & Toscano, 2009) Preparation MD simulations were conducted for 70 ns with no restraints (Figure 2). Steps (Cerliani et al., 2016; Lyons et al., 2015) used position restraints on all protein atoms. To ensure true NPT ensemble sampling during 70 ns preparation runs, the Velocity Rescale thermostat (Bussi et al., 2007) and Parrinello-Rahman barostat (Parrinello & Rahman, 1981) were used to maintain temperature and pressure, respectively. Time constants were 2.0 and 0.1 picoseconds for pressure and temperature coupling, respectively, utilizing the isothermal compressibility of water, 4.5^{-5} bar^{-1}. Box size for equilibration for the aglycosylated structure was $16.03422 \times 16.03422 \times 16.03422$ nm^3 with 397,857 water molecules, 804 ions, and 411,482 total atoms. Box size for equilibration for the glycosylated structure was $17.13643 \times 17.13643 \times 17.13643$ nm^3 with 486,735 water molecules, 974 ions, and 501,963 total atoms. All simulation steps used Particle Ewald Mesh algorithm(Ewald, 1921; Di Pierro et al., 2015) for long-range electrostatic calculations with cubic interpolation and 0.16 nm maximum grid spacing. Short-range nonbonded interactions were cut off at 1.0 nm. All water bond lengths were constrained with SETTLE (Miyamoto & Kollman, 1992) and the remaining bond lengths

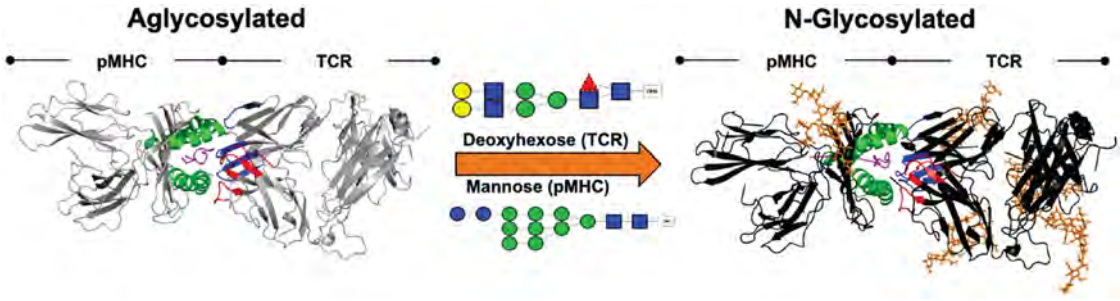

Figure 1. Graphic representation of N-Glycosylation of the DMF5 TCR bound to the MART1 restricted pMHC. The following interfacial substructures are highlighted: MHCα & MHCβ = green, TCR CDRα = blue, TCR CDRβ = red, MART1 peptide = magenta, glycans = orange, non-interacting body of aglycosylated structure = gray, and non-interacting body of glycosylated structure = black. The aglycosylated structure(left) was glycosylated (right) by attaching the deoxyhexose containing N-glycan (middle, top) to the TCR (N405, N497, N560, N568, and N765) and the high mannose containing N-glycan (middle bottom) to the pMHC (N86). Glycan representations align with the Consortium of Functional Glycomics nomenclature.

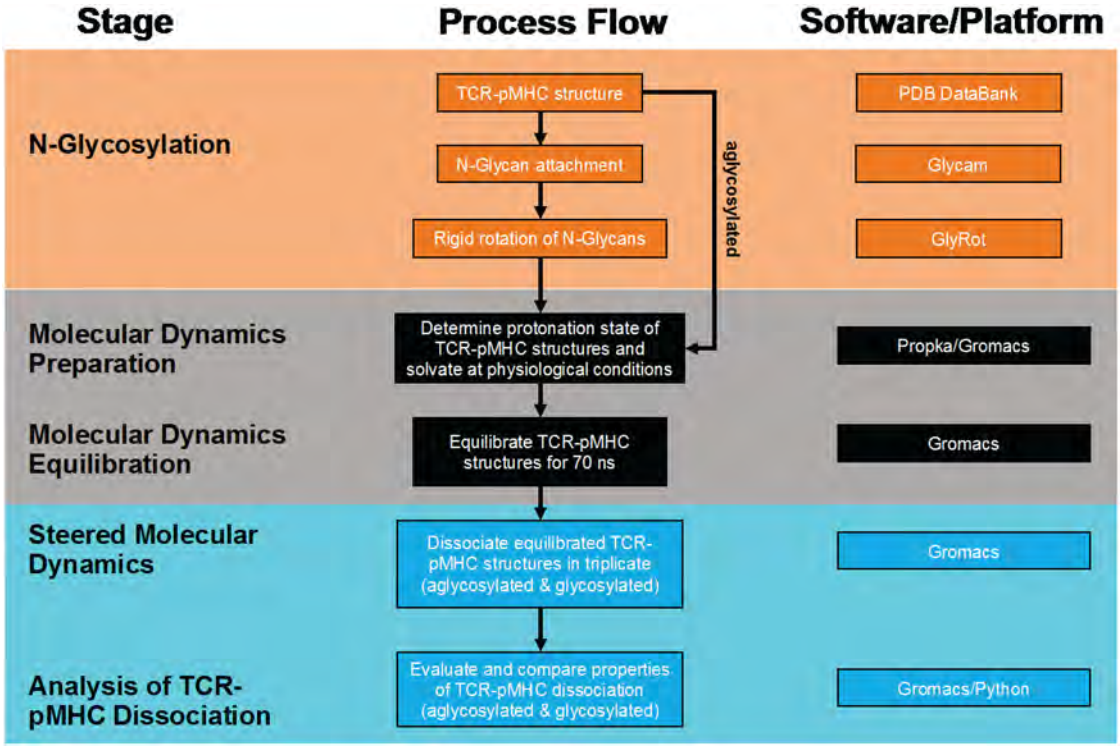

Figure 2. Process flow diagram for the evaluation of TCR-pMHC dissociation for aglycosylated and glycosylated structures. This includes the stage of the TCR-pMHCs (left column), the operation performed on the TCR-pMHC structures (middle column), and the software/platform used to perform operations (right column).

Table 1. Steered MD (SMD) simulations of aglycosylated and glycosylated structures including number of solvent molecules, number of ions, and total atoms in respective simulation boxes.

TCR-pMHC	Equilibration time (ns)	SMD water molecules	SMD ions	SMD total atoms
Aglycosylated	70	119,025	363 Na, 343 Cl	370,602
	60	119,003	363 Na, 343 Cl	370,536
	50	118,999	363 Na, 343 Cl	370,524
Glycosylated	70	118,592	363 Na, 343 Cl	370,736
	60	118,525	363 Na, 343 Cl	370,535
	50	118,555	363 Na, 343 Cl	370,625

were constrained using the LINCS algorithm. (Hess et al., 1997) Leap-frog algorithm was used for integrating Newton's equations of motion with 2 fs time steps. After 50, 60, and 70 ns, respectively, of the preparation run MD configurations for each peptide mutant were extracted and used as the three different starting points for steered molecular dynamics simulations.

Steered molecular dynamics (SMD)

The full protein structure was extracted for both glycosylated and aglycosylated cases at all preparation MD starting configurations (50, 60, 70 ns) (Figure 2). These protein complexes were aligned along the *x*-axis (supplementary material Figure S2A) and solvated in rectangular water boxes with dimensions

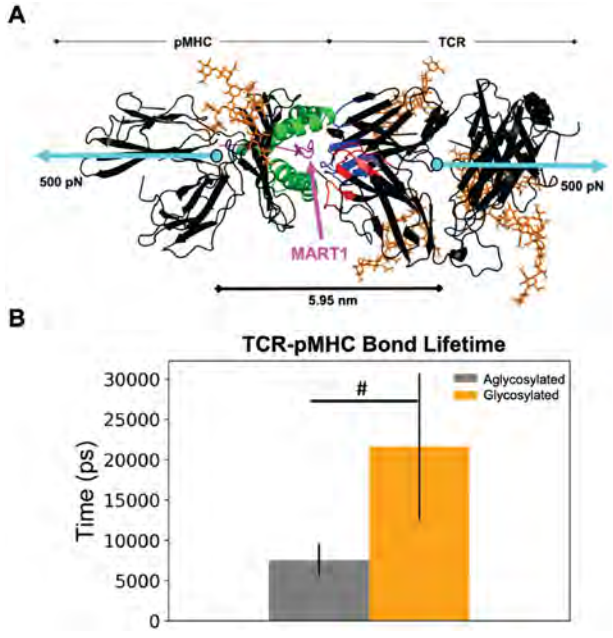

Figure 3. Graphic of steered molecular dynamic (SMD) simulations and TCR-pMHC bond lifetime. (A) The following interfacial substructures are highlighted: MHCα & MHCβ = green, TCR CDRα = blue, TCR CDRβ = red, MART1 peptide = magenta, glycans = orange, non-interacting body of aglycosylated structure = gray, and non-interacting body of glycosylated structure = black. Additionally, the pulling direction (cyan circles and arrows, respectively) and the position of and distance between COMs (scale bar at bottom). (B) Applying a constant force to the TCR-pMHC, we separated the aglycosylated (gray) and glycosylated (orange) structures and estimated the mean bond lifetime from three independent SMD simulations (70, 60, 50 ns starting configurations). Error represents SEM. The bond lifetimes were statistically compared with a one-tailed student's t-test: # $p \leq 0.10$.

$29.8 \times 9.9 \times 12.6\,nm^3$. As before, solvent is represented by the SPC/E water model and Na^+ and Cl^- ions were added to neutralize protein charge and reach physiologic salt concentration ~150 mM (Table 1). Before pulling, all systems underwent (Marth & Grewal, 2008) energy minimization (Lyons et al., 2015) 100 ps NVT (Bousser et al., 2020) and 100 ps NPT. During pull, the Nose-Hoover thermostat(Evans & Holian, 1985) and Parrinello-Rahman barostat (Parrinello & Rahman, 1981) were used to maintain temperature and pressure. A 500 pN linear potential (i.e., constant force) was applied to the center of mass (COM) of the TCR and pMHC along the *x*-direction (Figure 3) and simulations continued until the interaction energy between the TCR-pMHC was zero and the distance between COMs reached 0.49 times the box size. Bond lifetime is estimated as the amount of simulation time needed to meet these criteria. The TCR-pMHC bond is a physical bond between biomolecules and is considered broken when the interaction energy between the TCR-pMHC is zero. The magnitude of applied force represents current state-of-the-art SMD (Rollins et al., 2022; Sibener et al., 2018; Wu et al., 2019) and the COM was chosen as the site of applied force because pulling from the TCR and MHC termini results in artificial unfolding (Rollins et al., 2022). All simulation trajectories and selected frames were visualized using the Pymol Molecular Graphics System (Schrodinger, LLC).

Endpoints, data analysis, and statistical analysis

Data analysis was performed with the Gromacs suite (Van Der Spoel et al., 2005) (i.e., gmx make_ndx, gmx hbond, gmx rms, gmx rmsf, and gmx_energy), python packages for data handling and visualization (i.e. numpy (Harris et al., 2020), pandas (Mckinney, 2010), matplotlib (Hunter & Hunter, 2007), GromacsWrapper (Beckstein, 2021), scipy (SciPy 1.0 Contributors, 2020), and pingouin (Vallat, 2018), and custom python scripts (Figure 2). The geometry of a Lennard-Jones contact is defined as a distance less than 0.35 nm between atoms. The principal component analysis of the simulation trajectories was performed using the package MD analysis (Gowers et al., 2016; Michaud-Agrawal et al., 2011). Results were presented as mean ± SEM. As indicated in figures, statistics were performed in python using scipy for Student's *t*-tests, scipy for one-way analysis of variance (ANOVA), and pingouin for pairwise Tukey-HSD post-hoc tests. Detailed outputs of statistical analysis were written to excel and are provided in supporting material. Custom scripts relevant to the production of figures have been made available on a Github repository: https://github.com/zrollins/TCRglyco.git.

Results

Equilibration and force-dependent dissociation kinetics

After the attachment of glycans to the TCR and pMHC, we equilibrated the aglycosylated and glycosylated structures for 70 ns. The glycosylated structures are aligned and overlayed after 50, 60 and 70 ns of simulation time to reveal independent initial starting configurations (supporting material Figure S1). For these starting figurations, the glycans demonstrate flexibility with non-intersecting conformations (supporting material Figure S1). By evaluating root mean square deviation (RMSD) of the protein chains, the complexes both reached equilibrated configurations around 40 ns (supporting material Figure S2). To appropriately sample the ensemble of equilibrated configurations, we extracted and aligned the TCR-pMHC structures after 50, 60, and 70 ns of simulation time (supporting material Figure S2 A,B). Interestingly, glycosylation of the TCR-pMHC structure alters the conformation of MHC α-helices surrounding the MART1 peptide (supporting material Figure S2 Bi) and TCR substructures (supporting material Figure S2 Bii) independent of fluctuations. Steered molecular dynamics (SMD) simulations are commonly used to assess and compare the dissociation of protein-protein interactions (Huang et al., 2022; Izrailev et al., 1999; Rollins et al., 2022). All extracted configurations (50, 60, and 70 ns) of the aglycosylated and glycosylated structures were dissociated by applying a linear potential to the center of mass (COM) of the TCR and pMHC (Figure 3(A)). Remarkably, these structural alterations result in significantly slower dissociation kinetics for the glycosylated TCR-pMHC structure as shown by the mean simulated bond lifetime for the glycosylated (~21 ns) and aglycosylated (~7.5 ns) structures (Figure 3(B)).

Interaction energy

Glycans attached to the TCR and pMHC are not interacting with their respective counterpart and this is demonstrated by negligble

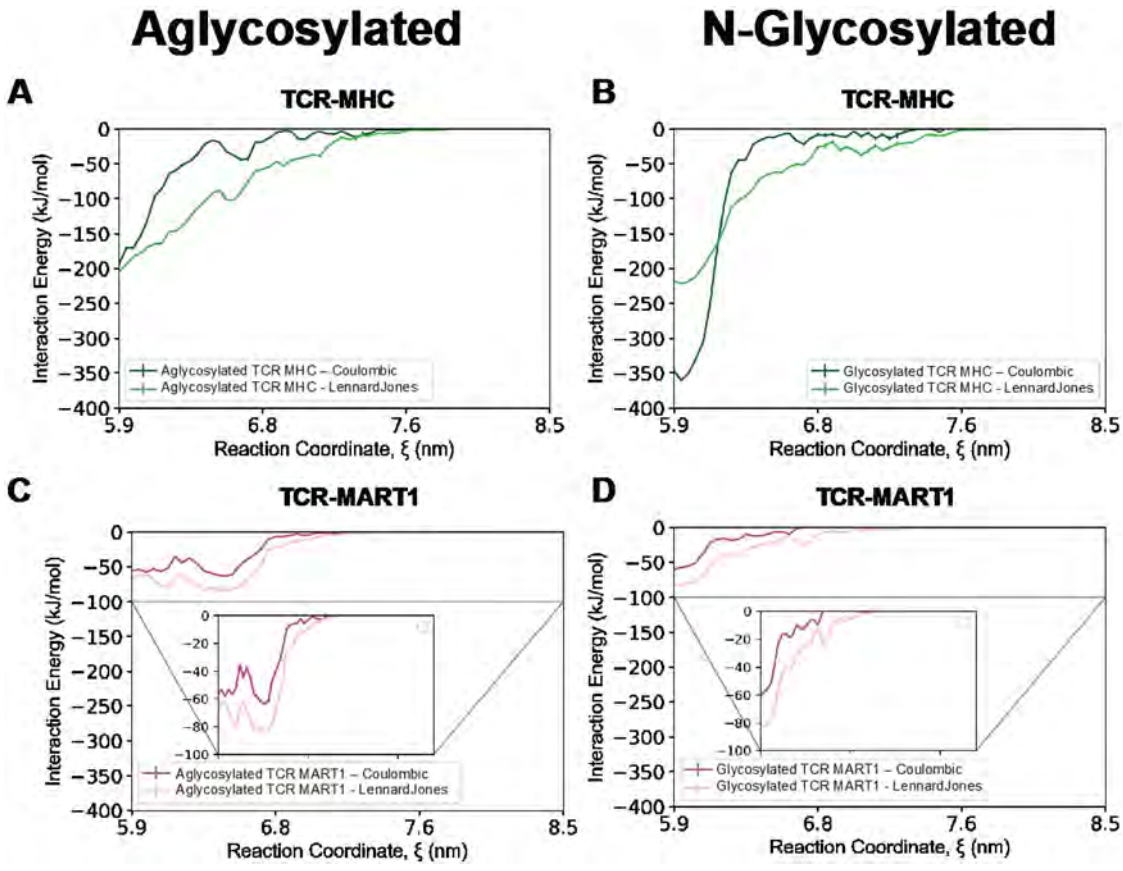

Figure 4. TCR-pMHC interaction energy. The interaction energy is separated into Lennard-Jones and Coulombic potential and plotted against the reaction coordinate (i.e., COM distance between the TCR and pMHC). This includes the interaction energy between TCR-MHC for the (A) aglycosylated (left, green) and (B) glycosylated structures (right, green). In addition, the interaction energy between TCR-MART1 for the (C) aglycosylated (left, pink) and (D) glycosylated structures (right, pink). For triplicate SMD simulations (70, 60, 50 ns), interaction energies were distributed into ~0.5 A bins and error represents SEM.

interaction energy (supporting material Figure S3) throughout the reaction coordinate (at least 100X less than protein-protein interactions) (Figure 4). Despite negligible energetic contributions from the glycan-protein or glycan-glycan interactions (supporting material Figure S3), the glycosylation induced structural alterations increase the interaction energy between the TCR-MHC and TCR-MART1 (Figure 4). For example, shifts in the MHC α-helices (supporting material Figure S2 Bi) result in an increased magnitude of coulombic interaction energy between TCR-MHC for the glycosylated structure (350 kJ/mol) compared to the aglycosylated structure (200 kJ/mol) at the initial reaction coordinate (Figure 4(A,B)). Moreover, shifts in the MART1 peptide and TCR (supporting material Figure S2 Bi-ii) result in an increased magnitude of Lennard-Jones interaction energy between the TCR-MART1 for the glycosylated structure (80 kJ/mol) compared to the aglycosylated structure (60 kJ/mol) at the initial reaction coordinate (Figure 4(C,D)).

Coulombic and Lennard-Jones interaction energies are dominated by hydrogen bonds (H-Bonds) and hydrophobic Lennard-Jones Contacts (LJ-Contacts), respectively. Thus, we quantified the number of H-bonds and LJ-contacts between the TCR-MHC and TCR-peptide. The interactions are categorized into low and high occupancy to compare the effect of transient and stabilized interactions, respectively. Occupancy is defined by the percentage of time under load the unique interaction exists in the SMD simulation. More low and high (up to 50%) occupancy H-Bonds between the TCR-MHC for the glycosylated structure (Figure 5(A)) agrees with the increased energetic strength of the glycosylated TCR-pMHC structure. Additionally, more total low and high occupancy (up to 50%) LJ-Contacts (Figure 5(B)) is consistent with increased energetic strength of the glycosylated TCR-pMHC structure.

Essential atomic motion of dissociation

We investigated the essential motion during dissociation to determine if increased TCR-pMHC bond strength was the result of differences in the equilibrated structures or conformational shifts under load. For both aglycosylated and glycosylated structures during the pull simulation, root mean square fluctuations do not exceed 0.10 nm for any TCR-pMHC substructure (Figure 6). There is only statistically significant difference in the CDR2α substructure fluctuation between aglycosylated and glycosylated structures. However, ~0.2 Å differences are unlikely to have physical significance. Furthermore, a principal component analysis on atomic motion indicates that more than 96% of essential atomic motion is in the direction of applied force (supporting material Figure S4) except for the 50 ns glycosylated configuration. Principal components 2-5 indicate that the TCR-pMHC interface is more energetically stabilized under load than the

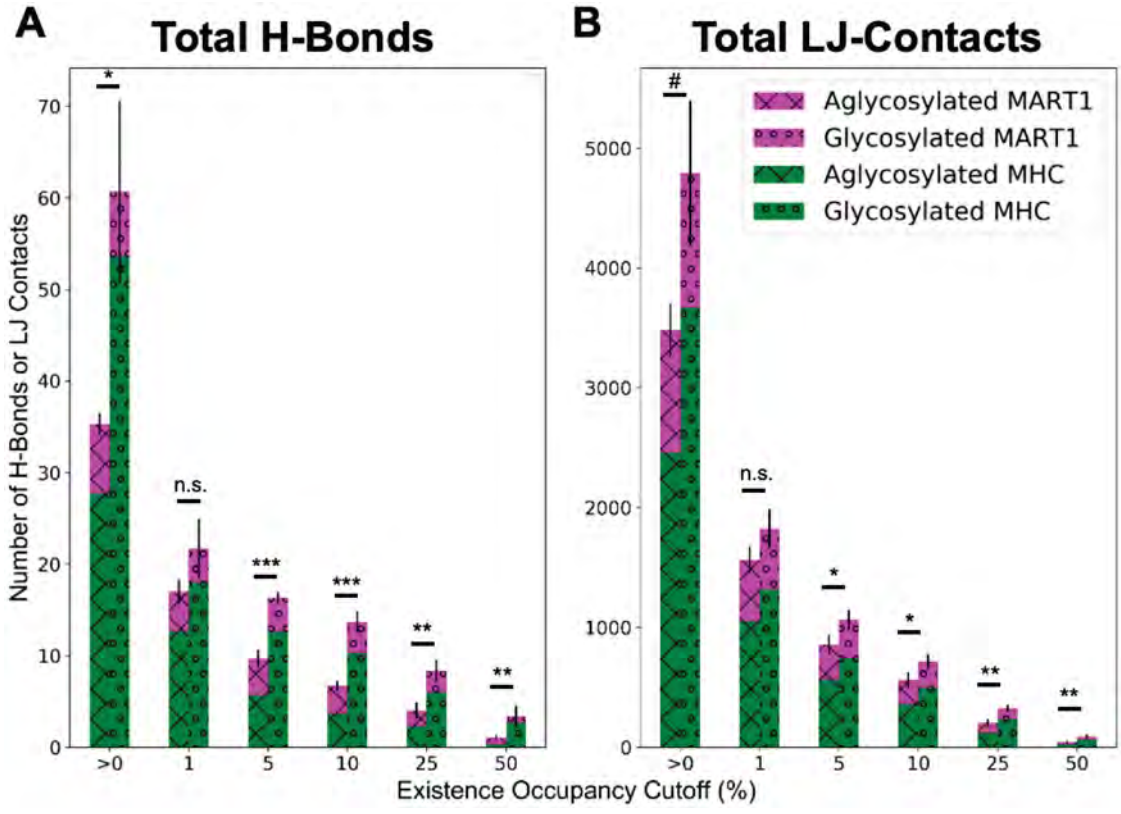

Figure 5. Hydrogen bonds and Lennard-Jones contacts. The number of unique interactions (H-bonds or LJ-contacts) are plotted with increasing existence occupancy and stacked: TCR-MART1 (magenta) stacked on TCR-MHC (green) interactions. This includes: (A) the number of unique H-bonds for the aglycosylated (crosses) and glycosylated (circles) structures (B) the number of unique LJ-Contacts for the aglycosylated (crosses) and glycosylated (circles) structures. Error represents SEM over three SMD simulations. The aglycosylated and glycosylated structures were statistically compared ($n = 3$): #$p < 0.10$, *$p < 0.05$, **$p < 0.01$, ***$p < 0.001$ by one-way ANOVA followed by Tukey-HSD post-hoc test.

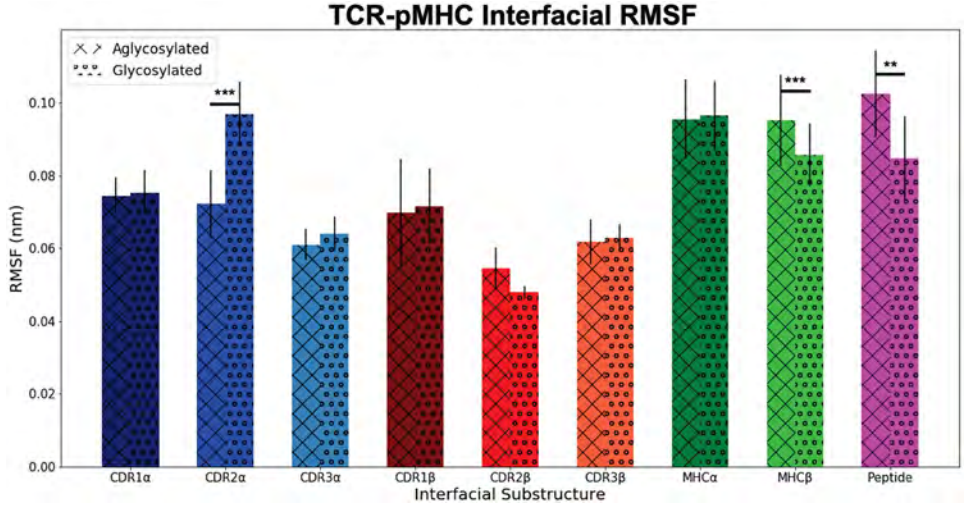

Figure 6. Interfacial substructure root mean square fluctuations (RMSF). The relative motion of the glycosylated (cross) and aglycosylated (circles) structures during SMD simulations are compared by calculating the RMSF at the TCR-pMHC interface. SMD error represents SEM on substructure atoms from three independent SMD simulations (70, 60, and 50 ns starting configurations). The glycosylated and aglycosylated substructures were statistically compared ($n = 3$): #$p < 0.10$, *$p < 0.05$, **$p < 0.01$, ***$p < 0.001$ by one-way ANOVA followed by Tukey-HSD post-hoc test.

quaternary structure of the TCR or pMHC, respectively (supporting material). Dominant atomic motion is in the direction of applied force (supporting material Figure S4) and comparable interfacial fluctuations (Figure 6) indicate that differences in bond strength are mostly attributed to differences in the equilibrated structures and not to conformational changes in the proteins during separation.

TCR-pMHC signature interaction maps

Existence maps of H-Bonds and LJ-Contacts were created for the aglycosylated and glycosylated structures to identify precise interactions that enhance bond strength. The H-Bond and LJ-Contact maps were created to include all interactions with greater than 5% and 80% existence occupancy,

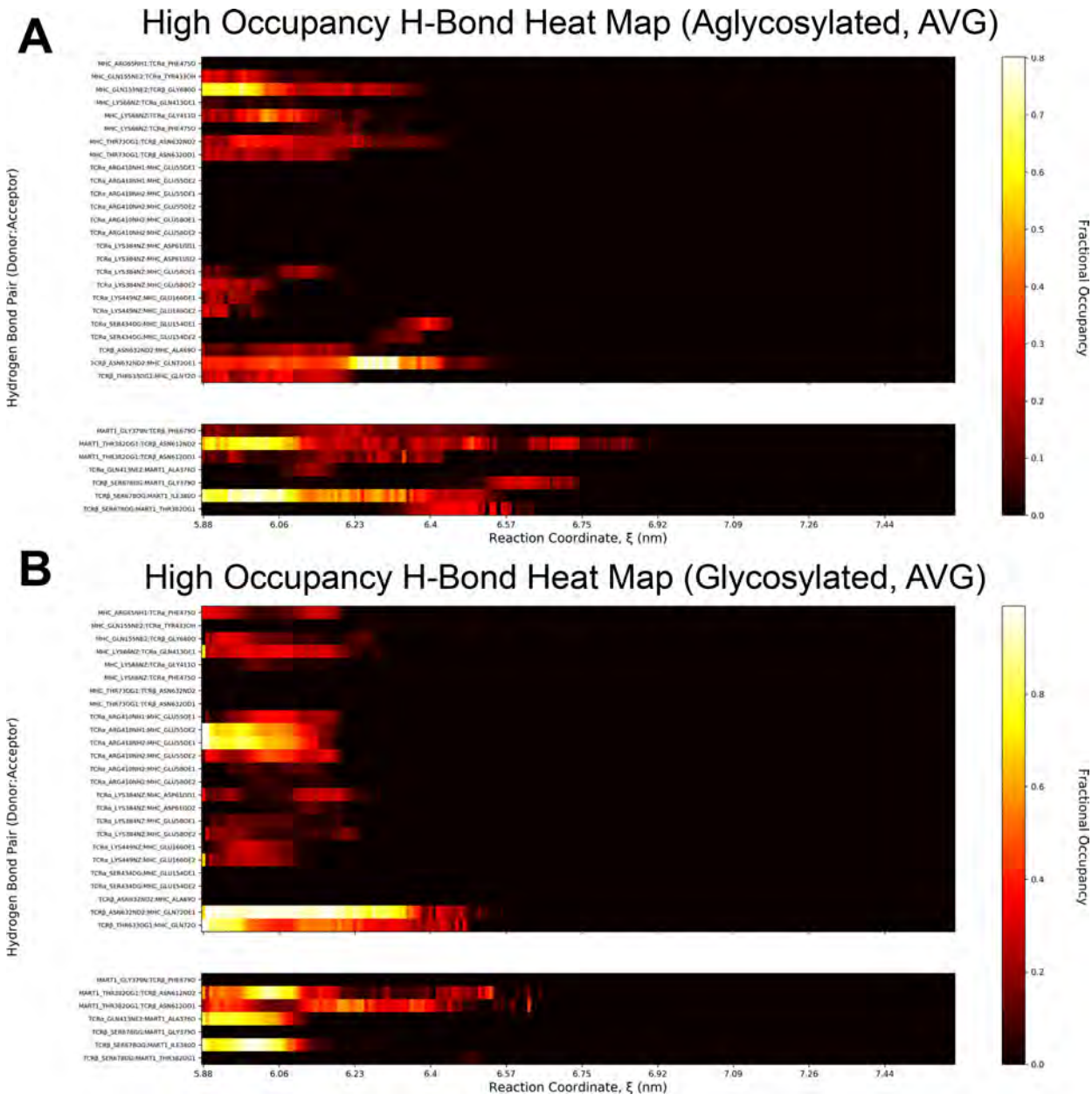

Figure 7. Average hydrogen bond existence maps as a function of reaction coordinate. The time axis of the existence maps is converted to COM distance by distributing time points into ~0.5 A bins and calculating the fractional occupancy in each respective bin. The 70, 60, 50 ns starting configurations for the (A) aglycosylated and (B) glycosylated structures are arithmetically averaged. The fractional occupancy of ~0.5 A bins is represented by the heat scale on the *y*-axis (right). The H-bond acceptor and donor are specified on the *y*-axis (left). The H-bonds are split into interactions between the TCR-MHC (top) and TCR-MART1 (bottom). For all interactions, H-bond donor-acceptor pairs with greater than 5% existence occupancy in at least 1/6 SMD simulations are included.

respectively, and located in at least one of the six SMD simulations. Additionally, the existence maps were plotted as a function of simulation time and the COM distance reaction coordinate for each SMD simulation (supporting material Figure S5–S8). Moreover, the TCR-MHC and TCR-MART1 interactions signatures were separated to be independently evaluated. The H-Bond maps as a function of reaction coordinate were averaged across the three equilibrated configurations for aglycosylated and glycosylated structures to reveal unique hydrogen bonding signatures (Figure 7). H-bond maps were chosen for display because of larger differences in energetics (Figure 4) and interactions (Figure 5) between the aglycosylated and glycosylated structures. The identical TCR-MHC and TCR-MART1 *y*-axis allows direct comparison between the aglycosylated and glycosylated structures and provide insight into the specific H-Bonds that may alter T-cell activation. For example, the donated H-Bond from TCR arginine 410 to MHC glutamic acid 155 is completely absent for all aglycosylated SMD configurations (Figure 7(B)), but present for all glycosylated configurations through ~6.2 nm of the reaction coordinate (Figure 7(A)). These detailed spatiotemporal interaction maps provide precise information on how glycosylation effects TCR-pMHC bond strength.

Discussion

The attachment of a deoxyhexose and high mannose containing N-glycans to the TCR and pMHC, respectively,

resulted in altered equilibrated TCR-pMHC structures. These altered structures impacted the strength of the TCR-pMHC bond including: the lifetimes, the energetic landscapes, and the atomic-level interactions.

N-glycosylation and TCR-pMHC structure

Investigation into the effects of N-glycosylation on TCR-pMHC structure, revealed that the equilibrated structure has altered conformation compared to the aglycosylated independent of fluctuations (supporting material Figure S2). This includes the MHC α-helices that surround the MART1 peptide (supporting material Figure S2 Bi) and the interacting substructures of the TCR (supporting material Figure S2 Bii). Since it is known that changes to the T cell glycome can affect T-cell activation (Sasawatari et al., 2020), the resulting alterations to the TCR-pMHC structure provide an intriguing hypothesis to explain biological behavior. Namely, we hypothesize that changes to the glycome will affect the N-glycosylation patterns on TCRs, the bond strength of TCR-pMHC interactions, and the activation signaling in T cells. However, future investigations will reveal the generalizability to other glycans and TCR-pMHC systems. Moreover, despite minimal atomic motion during dissociation at the TCR-pMHC interface (Figure 6 and supporting material Figure S4), alterations in the equilibrated structure following glycosylation resulted in enhanced overall bond strength (Figures 3–5) and atomic-level interaction signatures (Figure 7 and supporting material Figure S5-8). This extended force-dependent bond lifetime is entirely consistent with the experimental observation of enhanced antitumor activity of T cells expressing relatively high levels of deoxyhexose containing *N*-glycans (Sasawatari et al., 2020). The effect of T cell glycosylation patterns on the experimental TCR-pMHC force-dependent bond lifetime is an important area of future investigation. Removing of the N-glycans reduces the strength of the TCR-pMHC interaction which may result in lower observed experimental bond lifetimes and may reduce the ability of the TCR to discriminate pMHCs. These results suggest that metabolic regulation of the T cell glycome could result in allosteric regulation of TCR binding interactions with target pMHCs.

TCR-pMHC interactions and bond strength

During TCR-pMHC dissociation, the glycosylated structure had longer bond lifetime (Figure 3(B)), more energetic strength (Figure 4), and an increased number of interactions (Figure 5). These indications correspond and demonstrate that glycosylation effects the overall bond strength of the TCR-pMHC interaction. Moreover, these results are consistent with our previous reports indicating glycans can increase the strength of protein-protein interactions (Huang et al., 2022) and the increase in interaction strength corresponds with TCR-pMHC immunogenicity (Rollins et al., 2022). Interestingly, these changes in bond strength arise despite negligible energetic contributions from glycan-glycan or glycan-protein interactions (supporting material Figure S3). Thus, our results suggest that glycosylation of the TCR-pMHC interaction leads to conformational changes to the TCR and pMHC that impact their physiochemical interaction at baseline leading to alterations in bond strength. The changes in the detailed interaction H-bond maps (e.g., H-bond from TCR arginine 410 to MHC glutamic acid 155) provide additional insight into key locations of the TCR-pMHC that impact overall bond lifetime.

Conclusion

We have demonstrated the importance of glycosylation on TCR-pMHC structure, interactions, and dissociation kinetics. Moreover, these results suggest that changes to the T cell glycome impact the strength of interaction between the TCR and pMHC. The resultant changes in interaction strength may affect the ability of the TCR to discriminate pMHCs; and thus, this study reinforces the relevance of the glycome in the context of T-cell activation.

Disclosure statement

No potential conflict of interest was reported by the authors.

Funding

Simulations were performed on the hpc1/hpc2 clusters in the UC Davis, College of Engineering. BSH was partially supported by LLNL's LDRD program, under the auspices of the U.S. Department of Energy by Lawrence Livermore National Laboratory under Contract DE-AC52-07NA27344. ZAR was partially supported by startup funding to SCG from the Department of Biomedical Engineering.

Data availability statement

The starting configurations of SMD simulations for glycosylated and aglycosylated structures have been available on a Dryad repository: https://doi.org/10.25338/B8Q05W. Moreover, csv files with all interactions as well as high resolution (300 DPI) interaction maps have been added to the Dryad repository. In addition, the trajectories and principal component projected trajectories (PC1-PC3) have been compiled and uploaded to the repository. Custom python scripts relevant to the production of figures are available on Github repository: https://github.com/zrollins/TCRglyco.

Authors contribution

ZAR performed simulations, analyzed and interpreted the data, and wrote the manuscript. BSH performed simulations and edited the manuscript. SCG designed the experiments, analyzed and interpreted the data, and secured the funding. RF designed the experiments, analyzed and interpreted the data, wrote the manuscript, and secured funding and computer time.

References

Bause, E. (1983). Structural requirements of N-glycosylation of proteins. Studies with proline peptides as conformational probes. *The Biochemical Journal*, *209*(2), 331–336. https://doi.org/10.1042/BJ2090331

Beckstein, O. (2021). *GromacsWrapper*. https://doi.org/10.5281/zenodo.17901.

Berendsen, H. J. C., Grigera, J. R., & Straatsma, T. P. (1987). The missing term in effective pair potentials. *The Journal of Physical Chemistry*, *91*(24), 6269–6271. https://doi.org/10.1021/j100308a038

Berendsen, H. J. C., Postma, J. P. M., Van Gunsteren, W. F., Dinola, A., & Haak, J. R. (1984). Molecular dynamics with coupling to an external bath. *Journal of Chemical Physics.*, *81*(8), 3684–3690. https://doi.org/10.1063/1.448118

Bernardi, A. (2020). *GlyRot*. GitHub.

Bernardi, A., Faller, R., Reith, D., & Kirschner, K. N. (2019). ACPYPE update for nonuniform 1–4 scale factors: Conversion of the GLYCAM06 force field from AMBER to GROMACS. *SoftwareX*, *10*, 100241. https://doi.org/10.1016/j.softx.2019.100241

Bernardi, A., Huang, Y., Harris, B., Xiong, Y., Nandi, S., McDonald, K. A., & Faller, R. (2020). Development and simulation of fully glycosylated molecular models of ACE2-Fc fusion proteins and their interaction with the SARS-CoV-2 spike protein binding domain. *PLoS One*, *15*(8), e0237295. https://doi.org/10.1371/JOURNAL.PONE.0237295

Bernardi, A., Kirschner, K. N., & Faller, R. (2017). Structural analysis of human glycoprotein butyrylcholinesterase using atomistic molecular dynamics: The importance of glycosylation site ASN241. *PLoS One*, *12*(11), e0187994. https://doi.org/10.1371/JOURNAL.PONE.0187994

Borbulevych, O. Y., Santhanagopolan, S. M., Hossain, M., & Baker, B. M. (2011). TCRs used in cancer gene therapy cross-react with MART-1/Melan-A tumor antigens via distinct mechanisms. *Journal of Immunology (Baltimore, MD: 1950)*, *187*(5), 2453–2463. https://doi.org/10.4049/jimmunol.1101268

Bousser, E. D., Meuris, L., Callewaert, N., & Festjens, N. (2020). Human T cell glycosylation and implications on immune therapy for cancer. *Human Vaccines & Immunotherapeutics*, *16*(10), 2374–2388. https://doi.org/10.1080/21645515.2020.1730658

Bussi, G., Donadio, D., & Parrinello, M. (2007). Canonical sampling through velocity rescaling. *The Journal of Chemical Physics*, *126*(1), 014101. https://doi.org/10.1063/1.2408420

Cerliani, J. P., Blidner, A. G., Toscano, M. A., Croci, D. O., & Rabinovich, G. A. (2016). Translating the 'sugar code'into immune and vascular signaling programs. *Trends in biochemical sciences*, *42*(4), 255–273.

Clark, M. C., & Baum, L. G. (2012). T cells modulate glycans on CD43 and CD45 during development and activation, signal regulation, and survival. *Annals of the New York Academy of Sciences, 1253*(1), 58–67.

D. A., Case, R. M., Betz, D. S., Cerutti, T. E., Cheatham, III, T. A., Darden, R. E., Duke, T. J., Giese, H. G., A. W., Goetz, N., Homeyer, S., Izadi, P., Janowski, J., Kaus, A., Kovalenko, T. S., Lee, S., LeGrand, P., Li, C., Lin, T., Luchko, R., Luo, … Kollman, P. A. (2016). *AMBER 2016*. University of California.

Evans, D. J., & Holian, B. L. (1985). The nose–hoover thermostat. The Journal of chemical physics, 83(8), 4069–4074.

Ewald, P. P. (1921). Die Berechnung optischer und elektrostatischer Gitterpotentiale. *Annalen Der Physik*, *369*(3), 253–287.

Gómez-Henao, W., Tenorio, E. P., Sanchez, F. R. C., Mendoza, M. C., Ledezma, R. L., & Zenteno, E. (2021). Relevance of glycans in the interaction between T lymphocyte and the antigen presenting cell. *International Reviews of Immunology*, *40*(4), 274–288. https://doi.org/10.1080/08830185.2020.1845331

Gowers, R.J., Linke, M., Barnoud, J., Reddy, T.J., Melo, M.N., Seyler, S.L., Domanski, J., Dotson, D.L., Buchoux, S., Kenney, I.M. and Beckstein, O. (2016). MDAnalysis: a Python package for the rapid analysis of molecular dynamics simulations. In *Proceedings of the 15th python in science conference* (Vol. 98, p. 105). Austin, T X: SciPy.

Grant, O. C., Montgomery, D., Ito, K., & Woods, R. J. (2020). 3D Models of glycosylated SARS-CoV-2 spike protein suggest challenges and opportunities for vaccine development. *bioRxiv*, 2020.04.07.030445. https://doi.org/10.1101/2020.04.07.030445

Group of Robert J. Woods. *GLYCAM Web*. Complex Carbohydrate Research Center, University of Georg Athens.

Harbison, A., & Fadda, E. (2020). An atomistic perspective on antibody-dependent cellular cytotoxicity quenching by core-fucosylation of IgG1 Fc N-glycans from enhanced sampling molecular dynamics. *Glycobiology*, *30*(6), 407–414. https://doi.org/10.1093/GLYCOB/CWZ101

Harris, C. R., Millman, K. J., van der Walt, S. J., Gommers, R., Virtanen, P., Cournapeau, D., Wieser, E., Taylor, J., Berg, S., Smith, N. J., Kern, R., Picus, M., Hoyer, S., van Kerkwijk, M. H., Brett, M., Haldane, A., Del Río, J. F., Wiebe, M., Peterson, P., … Oliphant, T. E. (2020). Array programming with NumPy. *Nature*, *585*(7825), 357–362. https://doi.org/10.1038/s41586-020-2649-2

Hess, B., Bekker, H., Berendsen, H. J. C., & Fraaije, J. G. E. M. (1997). LINCS: A linear constraint solver for molecular simulations. *Journal of Computational Chemistry*, *18*(12), 1463–1472. https://doi.org/10.1002/(SICI)1096-987X(199709)18:12<1463::AID-JCC4>3.0.CO;2-H

Huang, Y., Harris, B. S., Minami, S. A., Jung, S., Shah, P. S., Nandi, S., McDonald, K. A., & Faller, R. (2022). SARS-CoV-2 spike binding to ACE2 is stronger and longer ranged due to glycan interaction. *Biophysical Journal*, *121*(1), 79–90. doi:10.1016/J.BPJ.2021.12.002/ATTACHMENT/E0AAE14F-B973-4AF5-B979-63C0E546FA4C/MMC1.PDF

Hunter, J. D., & Hunter, D. (2007). Matplotlib: A 2D graphics environment. *Computing in Science & Engineering*, *9*(3), 90–95. https://doi.org/10.1109/MCSE.2007.55

Izrailev, S., Stepaniants, S., Isralewitz, B., Kosztin, D., Lu, H., Molnar, F., Wriggers, W., & Schulten, K. (1999). Steered molecular dynamics. In *Computational molecular dynamics: challenges, methods, ideas* (pp. 39-65). Berlin, Heidelberg: Springer.

Jo, S., Qi, J., & Im, W. (2015). Preferred conformations of N-glycan core pentasaccharide in solution and in glycoproteins. *Glycobiology*, *26*, cwv083–cwv29. https://doi.org/10.1093/glycob/cwv083

Kirschner, K. N., Yongye, A. B., Tschampel, S. M., González-Outeiriño, J., Daniels, C. R., Foley, B. L., & Woods, R. J. (2008). GLYCAM06: A generalizable biomolecular force field. Carbohydrates. *Journal of Computational Chemistry*, *29*(4), 622–655. https://doi.org/10.1002/JCC.20820

Lu, D., Yang, C., & Liu, Z. (2012). How hydrophobicity and the glycosylation site of glycans affect protein folding and stability: A molecular dynamics simulation. *The Journal of Physical Chemistry B*, *116*(1), 390–400. https://doi.org/10.1021/jp203926r

Lyons, J. J., Milner, J. D., & Rosenzweig, S. D. (2015). Glycans instructing immunity: The emerging role of altered glycosylation. *Frontiers in Pediatrics*, *3*, 54. doi:10.3389/FPED.2015.00054

Maier, J. A., Martinez, C., Kasavajhala, K., Wickstrom, L., Hauser, K. E., & Simmerling, C. (2015). ff14SB: Improving the accuracy of protein side chain and backbone parameters from ff99SB. *Journal of Chemical Theory and Computation*, *11*(8), 3696–3713. https://doi.org/10.1021/ACS.JCTC.5B00255

Marth, J. D., & Grewal, P. K. (2008). Mammalian glycosylation in immunity. *Nature Reviews. Immunology*, *8*(11), 874–887. *2008 811* https://doi.org/10.1038/nri2417

Mckinney, W. (2010). *Data structures for statistical computing in Python* [Paper presentation]. In *Proceedings of the 9th Python in Science Conference* (Vol. 445, No. 1, pp. 51-56), Austin, Texas.

Michaud-Agrawal, N., Denning, E. J., Woolf, T. B., & Beckstein, O. (2011). MDAnalysis: A toolkit for the analysis of molecular dynamics simulations. *Journal of Computational Chemistry*, *32*(10), 2319–2327.

Miyamoto, S., & Kollman, P. A. (1992). Settle: An analytical version of the SHAKE and RATTLE algorithm for rigid water models. *Journal of Computational Chemistry*, *13*(8), 952–962. https://doi.org/10.1002/jcc.540130805

Olsson, M. H. M., SØndergaard, C. R., Rostkowski, M., & Jensen, J. H. (2011). PROPKA3: Consistent treatment of internal and surface residues in empirical pKa predictions. *Journal of Chemical Theory and Computation*, *7*(2), 525–537. https://doi.org/10.1021/ct100578z

Parrinello, M., & Rahman, A. (1981). Polymorphic transitions in single crystals: A new molecular dynamics method. *Journal of Applied Physics.*, *52*(12), 7182–7190. https://doi.org/10.1063/1.328693

Petrescu, A. J., Petrescu, S. M., Dwek, R. A., & Wormald, M. R. (1999). A statistical analysis of N- and O-glycan linkage conformations from crystallographic data. *Glycobiology*, *9*(4), 343–352. https://doi.org/10.1093/GLYCOB/9.4.343

Di Pierro, M., Elber, R., & Leimkuhler, B. (2015). A stochastic algorithm for the isobaric–isothermal ensemble with Ewald summations for all long range forces. *Journal of chemical theory and computation*, 11(12), 5624–5637.

Rabinovich, G. A., & Toscano, M. A. (2009). Turning "sweet" on immunity: galectin–glycan interactions in immune tolerance and inflammation.

Nature Reviews. Immunology, *9*(5), 338–352. *2009 95* https://doi.org/10.1038/nri2536

Rollins, Z. A., Faller, R., & George, S. C. (2022). Using molecular dynamics simulations to interrogate T cell receptor non-equilibrium kinetics. *Computational and Structural Biotechnology Journal*, *20*, 2124–2133.

Rollins, Z. A., Huang, J., Tagkopoulos, I., Faller, R., & George, S. C. (2021). The atomic-level physiochemical determinants of T cell receptor dissociation kinetics. *BioRxiv*, 2021.10.25.465739. https://doi.org/10.1101/2021.10.25.465739

Ryan, S. O., & Cobb, B. A. (2012). Roles for major histocompatibility complex glycosylation in immune function. *Seminars in Immunopathology*, *34*(3), 425–441. https://doi.org/10.1007/S00281-012-0309-9

Sasawatari, S., Okamoto, Y., Kumanogoh, A., & Toyofuku, T. (2020). Blockade of N-glycosylation promotes antitumor immune response of T cells. *Journal of Immunology (Baltimore, MD : 1950)*, *204*(5), 1373–1385. https://doi.org/10.4049/JIMMUNOL.1900937

Schjoldager, K. T., Narimatsu, Y., Joshi, H. J., & Clausen, H. (2020). Global view of human protein glycosylation pathways and functions. *Nature Reviews. Molecular Cell Biology*, *21*(12), 729–749. *2020 2112* https://doi.org/10.1038/s41580-020-00294-x

Sibener, L. V., Fernandes, R. A., Kolawole, E. M., Carbone, C. B., Liu, F., McAffee, D., Birnbaum, M. E., Yang, X., Su, L. F., Yu, W., Dong, S., Gee, M. H., Jude, K. M., Davis, M. M., Groves, J. T., Goddard, W. A., Heath, J. R., Evavold, B. D., Vale, R. D., & Garcia, K. C. (2018). Isolation of a structural mechanism for uncoupling T cell receptor signaling from peptide-MHC binding. *Cell*, *174*(3), 672–687.e27. https://doi.org/10.1016/j.cell.2018.06.017

Søndergaard, C. R., Olsson, M. H. M., Rostkowski, M., & Jensen, J. H. (2011). Improved treatment of ligands and coupling effects in empirical calculation and rationalization of pKa values. *Journal of Chemical Theory and Computation*, *7*(7), 2284–2295. https://doi.org/10.1021/ct200133y

Sousa da Silva, A. W., & Vranken, W. F. (2012). ACPYPE - AnteChamber PYthon Parser interfacE. *BMC Research Notes*, *5*(1), 1–8. *2012 51* https://doi.org/10.1186/1756-0500-5-367

Vallat, R. (2018). Pingouin: Statistics in Python. *Journal of Open Source Software*, *3*(31), 1026. https://doi.org/10.21105/joss.01026

Van Der Spoel, D., Lindahl, E., Hess, B., Groenhof, G., Mark, A. E., & Berendsen, H. J. C. (2005). GROMACS: Fast, flexible, and free. *Journal of Computational Chemistry*, *26*(16), 1701–1718. https://doi.org/10.1002/jcc.20291

Virtanen, P., Gommers, R., Oliphant, T. E., Haberland, M., Reddy, T., Cournapeau, D., Burovski, E., Peterson, P., Weckesser, W., Bright, J., van der Walt, S. J., Brett, M., Wilson, J., Millman, K. J., Mayorov, N., Nelson, A. R. J., Jones, E., Kern, R., Larson, E., … van Mulbregt, P., SciPy 1.0 Contributors (2020). SciPy 1.0: Fundamental algorithms for scientific computing in Python. *Nature Methods*, *17*(3), 261–272. *2020 173* https://doi.org/10.1038/s41592-019-0686-2

Woo, H., Park, S.-J., Choi, Y. K., Park, T., Tanveer, M., Cao, Y., Kern, N. R., Lee, J., Yeom, M. S., Croll, T. I., Seok, C., & Im, W. (2020). Developing a fully glycosylated full-length SARS-CoV-2 spike protein model in a viral membrane. *The Journal of Physical Chemistry. B*, *124*(33), 7128–7137. https://doi.org/10.1021/ACS.JPCB.0C04553

Wooster, A. L., Anderson, T. S., & Lowe, D. B. (2019). Expression and characterization of soluble epitope-defined major histocompatibility complex (MHC) from stable eukaryotic cell lines. *Journal of Immunological Methods*, *464*, 22–30. https://doi.org/10.1016/J.JIM.2018.10.006

Wu, P., Zhang, T., Liu, B., Fei, P., Cui, L., Qin, R., Zhu, H., Yao, D., Martinez, R. J., Hu, W., An, C., Zhang, Y., Liu, J., Shi, J., Fan, J., Yin, W., Sun, J., Zhou, C., Zeng, X., … Lou, J. (2019). Mechano-regulation of peptide-MHC class I conformations determines TCR antigen recognition. *Molecular Cell*, *73*(5), 1015–1027.e7. https://doi.org/10.1016/j.molcel.2018.12.018

Xiong, Y., Karuppanan, K., Bernardi, A., Li, Q., Kommineni, V., Dandekar, A. M., Lebrilla, C. B., Faller, R., McDonald, K. A., & Nandi, S. (2019). Effects of N-glycosylation on the structure, function, and stability of a plant-made fc-fusion anthrax decoy protein. *Frontiers in Plant Science*, *10*, 768. doi:10.3389/fpls.2019.00768

Yanaka, S., Yogo, R., Inoue, R., Sugiyama, M., Itoh, S. G., Okumura, H., Miyanoiri, Y., Yagi, H., Satoh, T., Yamaguchi, T., & Kato, K. (2019). Dynamic views of the Fc region of immunoglobulin G provided by experimental and computational observations. *Antibodies*, *8*(3), 39. https://doi.org/10.3390/antib8030039